Supporting information (SI)

Mercury stable isotopes discriminate different populations of European seabass and trace potential Hg sources around Europe

Alice Cransveld*[,a], David Amouroux[b], Emmanuel Tessier[b], Emmanuil Koutrakis[c], Ayaka A Ozturk[d], Nicola Bettoso[e], Nicolas Sturaro[a], Cláudia L. Mieiro[f], Sylvain Bérail[b], , Julien P. G. Barre[b], Joseph Schnitzler[a,g], Krishna Das*[,a]

a. Laboratory for Oceanology-MARE, University of Liège, 15 Allée du 6 Août, 4000 Liège, Belgium

b. CNRS/ UNIV PAU & PAYS ADOUR, Institut des Sciences Analytiques et de Physico-Chimie pour l'Environnement et les Materiaux, UMR5254, 64000, PAU, France

c. Fisheries Research Institute, Hellenic Agricultural Organisation, 640 07 Nea Peramos, Kavala, Greece

d. Faculty of Fisheries, Istanbul University, Turkey

e. Agenzia Regionale per la Protezione dell'Ambiente del Friuli Venezia Giulia (ARPA FVG), via A. La Marmora 13, 34139 Trieste, Italy

f. CESAM and Departamento de Biologia, Universidade de Aveiro, Campus Universitário de Santiago, 3810-193 Aveiro, Portugal

g. Institute for Terrestrial and Aquatic Wildlife Research, University of Veterinary Medicine Hannover, Foundation, 25761 Büsum, Schleswig-Holstein, Germany.

Pages: 21

Figures: 16

Tables: 9

Material and method:

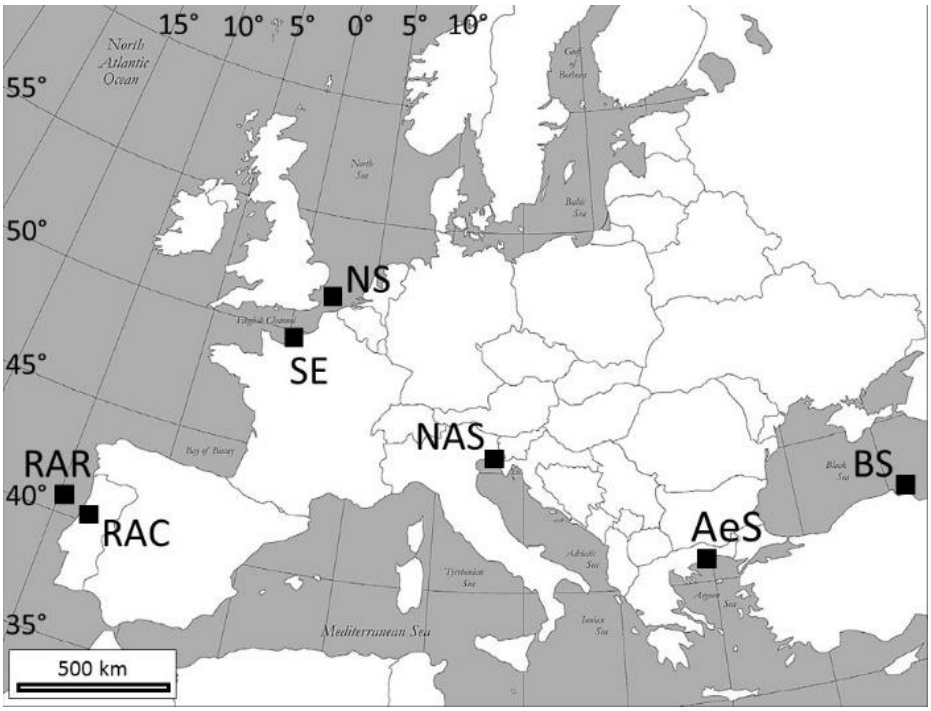

Figure S-1 : Sampling sites of *Dicentrarchus labrax:* The North Sea (NS), the Aegean Sea (AeS), the Seine estuary (SE), the Northern Adriatic Sea (NAS), the Black Sea (BS), and two different sites at the Ria de Aveiro lagoon in Portugal: the reference site, RAR and the contaminated site RAC. (map source: Cartographic Research Lab, University of Alabama)

Site description

Both NS and SE sites are located in the the Greater North Sea which undergoes eutrophication and massive anthropogenic pressures, with mercury levels posing serious environmental risks in some coastal areas sediments[1]. The Seine Estuary and Bay are some of the most metal contaminated marine areas in Europe because of intensive industrial activity in the hinterland, coupled to a dense population in the River Basin[2].

The AeS site is in the Agiasma lagoon, Kavala Gulf, Greece. It is part of the Nestos Delta area, protected by the Ramsar convention[3]. Although the Kavala Gulf is regarded as a hotspot of pollution, the Agiasma lagoon sediments show lower Hg contamination compared to polluted lagoons and coastal ecosystems of the Mediterranean Sea[3].

The BS samples were taken along the coast between the towns Sinop and Gerze. Scarce information is available on mercury sources and levels in the Black Sea[4]. Because of its semi-enclosed basin, and the many rivers that discharge into it, the unrestricted shipping, mineral exploitation, the dumping of toxic wastes, and the discharge of domestic wastes from coastal cities, the BS has suffered from extensive pollution[5]. Moreover, ninety percent of its water mass is anoxic[5–8], raising concerns about possible high levels of Hg methylation.

The NAS samples were collected in the lagoon of Marano and Grado in the Gulf of Trieste, one of the most contaminated areas in the Mediterranean basin. The former Idrija mercury mine (western Slovenia), has been the world's second largest Hg mining area. It dumped cinnabar residues along the Idrijca River and Hg was transported downstream to the Adriatic Sea through the Gulf of Trieste and to the lagoon where Hg

concentrations in sediments remain high[9]. In addition the Lagoon experienced the input from a chlor-alkali plant, when Hg was discharged in an uncontrolled manner from 1949 to 1984[10].

The Ria de Aveiro is a lagoon that has been subjected to Hg effluents from a chlor-alkali plant for almost five decades (1950–1994) and high Hg concentrations are still associated to sediments[11,12]. Sampling was performed between 2009 and 2012 at Laranjo Basin at two sites: RAC was near the Hg source and recognized as a highly contaminated area, and RAR was near the lagoon outlet, 10 km seaward from the pollution source and considered as a reference area[11]

Stomach content analysis

During dissection of the sampled fish, we also looked at stomach content. We counted and identified the preys to the most precise level possible with a binocular. Not all stomachs contained preys.

Table S-1 : Importance of prey taxa in all analysed stomachs of *Dicentrarchus labrax*. n is the number of stomachs analysed, O is the occurrence of prey (the number of stomach where we observed them) , and N is the total number of prey (summing every prey observed in all stomachs).

Site	n	Number of empty stomachs	Prey taxa	O	N
Agean Sea	8	2	Teleost fish	2	2
			Crustacean	5	45
			Gammarus sp.	3	20
			Isopod	1	20
			Copepod	1	2
			Crabs sp	1	1
North Sea	0	/	/	/	/
Seine Estuary	10	3	Teleost fish	1	1
			Annelida polychaeta	1	1
			Crusteacea	7	19
			Amphipoda spp.	1	2
			Liocarcinus holsatus	2	3
			Liocarcinus pusillus	1	1
			Liocarcinus sp.	2	2
			Pilumnus hirtellus	2	2
			Crabs spp.	4	6
Black sea	10	8	Crustacea	2	2
			Shrimp spp.	2	2
Northern Adriatic Sea	9	2	Teleost fish	5	5
			Crustacean	6	17
			Crangon crangon	2	11
			Shrimp spp.	3	3
			Crabs sp	1	1
Rio de Aveiro Ref.	10	2	Teleost fish	1	1
			Annelida polychaeta	2	2
			Crusteacea	6	13

			Isopoda	1	1
			Shrimp spp.	2	5
			Crabs spp.	4	5
			Algae	1	1
Rio de Aveiro Cont.	12	0	Annelida polychaeta	5	9
			Crusteacea	10	19
			Shrimp spp.	5	9
			Crabs spp.	7	10

Analytical procedures

Nitrogen (N) and carbon (C) isotopes are useful tools to characterize diets and trophic niches[13,14]. Stable isotope ratios of carbon ($^{13}C/^{12}C$) and nitrogen ($^{15}N/^{14}N$) were determined with an isotope ratio mass spectrometer (IsoPrime100, Isoprime, UK) coupled in continuous flow to an elemental analyzer (vario MICRO cube, Elementar, Germany). Reference materials (IAEA CH-6 and IAEA-N2) were analyzed to insure the precision and quality of the analyses. Stable isotope ratios are expressed in delta notation, $\delta^{13}C$ and $\delta^{15}N$, as part per thousand. Carbon and nitrogen ratios are expressed relative to the V-PDB (Vienna Peedee Belemnite) standard and to atmospheric nitrogen, respectively. The precision of replicate analyses were within 0.1 ‰ for $\delta^{13}C$ and 0.3 ‰ for $\delta^{15}N$.

In order to allow inter-population comparison, we also calculated each individual's trophic level (TL) using the following equation, after Post[13]:

$$TL = \lambda + \frac{(\delta^{15}N_{sample} - \delta^{15}N_{baseline})}{TEF} \qquad (1)$$

where TEF is the trophic enrichment factor, estimated around 2.54 after Vanderklift[15], and λ is the estimated trophic level of the baseline. $\delta^{15}N$ values for baselines of sampling sites were found in literature[16–21]. We preferentially used primary consumers such as bivalves for $\delta^{15}N$ baseline values, as they are ecological integrators, and assigned them a λ=2. However, when data was unavailable for this trophic level, we used POM $\delta^{15}N$, and we assigned POM a λ=1.5, to take into account that there are not only primary producers in POM[22,23].

Total Hg (THg) concentrations were determined directly on powder samples by atomic absorption spectrometry (AAS) on a Milestone Direct Mercury Analyzer 80 (DMA-80, Milestone). The method has been validated for solid samples using US EPA Method 7473. Quality assurance methods included evaluating by measuring blanks, standard solutions, triplicates of samples, and certified reference material NRC-DORM-2. Recovery of THg in CRM (9 replicates) ranged from 89% to 110%, averaging 99 ± 6% (Table S-2). T-Hg concentration is expressed ng.g^{-1} dry weight (DW).

Table S-2 : Total Hg concentration in certified reference material. Comparison of certified and obtained values on Direct Mercury Analyser. Results are expressed as mean values ± 1SD (standard deviation).

CRM	n	THg			
		obtained	certified	Certified corrected for 0,056% humidity	recovery
		$ng \cdot g^{-1}$	$ng \cdot g^{-1}$	$ng \cdot g^{-1}$	%
DORM-2	9	4353 ± 269	4640 ± 260	4379 ± 245	99 ± 6

Methylmercury and inorganic Hg concentrations were determined by isotope dilution-gas chromatography-inductively coupled plasma-mass spectrometer (ID-GC-ICP-MS) following microwave-assisted extraction and aqueous phase derivatization[24]. For the extraction, about 100mg of sample were weighted and 3 to 5ml of tetramethylamonium hydroxide (TMAH) was added. After microwave extraction, ^{199}IHg and ^{201}MHg spikes were added for isotope dilution, and sodium tetraethylborate as derivatizing agent, then samples were introduced in GC-ICP-MS. Measures were performed in triplicates. The sum of IHg and MeHg was compared with THg analysis (DMA-80) to verify the recovery of the extraction, which was 90 ± 10 % on average. Reference material included BCR CRM-464 (tuna fish muscle, from Adriatic Sea, certified for MeHg and THg concentration), and DOLT-4 (dogfish liver) (Table S-3).

Table S-3 : Hg speciation in certified reference materials. Comparison of certified and obtained values on GC-ICP-MS. Results are expressed as mean values ± 1SD (standard deviation).

CRM	n	THg			MeHg			MHg/tot		
		obtained	certified	recovery	obtained	certified	recovery	obtained	certified	recovery
		$ng \cdot g^{-1}$	$ng \cdot g^{-1}$	%	$ng \cdot g^{-1}$	$ng \cdot g^{-1}$	%	%	%	%
BCR 464	7	4438 ± 586	5240 ± 100	85 ± 11	4260 ± 540	5120 ± 171	83 ± 11	96 ± 1	98 ± 3	98 ± 1
DOLT 4	2	2189 ± 337	2580 ± 220	85 ± 13	1130 ± 113	1330 ± 120	85 ± 8	52 ± 3	52 ± 5	101 ± 6

Mercury isotopic composition analysis was performed using cold vapor generation (CVG) with multi-collector-inductively coupled plasma-mass spectrometer (MC-ICP-MS, Nu Instruments). First, between 50 and 500 mg of muscle samples were mineralized in quartz vials with high purity nitric acid (HNO_3), using a High Pressure Asher (HPA). Hydrogen peroxide (H_2O_2) was then added and samples went through digestion process for three more hours on a hot block (80°C). Samples were introduced to the ICP as a Hg0 cold vapor by reduction of Hg(II) with $SnCl_2$ in a custom quartz gas liquid separator. We performed analysis of samples on MC-ICP-MS for the six most abundant Hg stable isotopes (^{198}Hg, ^{199}Hg, ^{200}Hg, ^{201}Hg, ^{202}Hg, and ^{204}Hg). A desolvation nebulisation system from Nu Instrument was used to introduce NIST-SRM-997 thallium for instrumental mass-bias correction using the exponential fractionation law. Reference material UM-Almaden and BCRCRM-464 were used as secondary standards (Table S-4). We used a standard-sample bracketing system to calculate δ values (in ‰) relative to the reference standard NIST SRM 3133 mercury spectrometric solution. Isotope ^{198}Hg was used as the reference for ratio determination of all other Hg isotopes, using the following equations:

$$\delta^{xxx}\mathrm{Hg} = [\frac{(^{xxx}\mathrm{Hg}/^{198}\mathrm{Hg})_{\mathrm{sample}}}{(^{xxx}\mathrm{Hg}/^{198}\mathrm{Hg})_{\mathrm{NIST\ 3133}}} - 1)] \times 1000 \qquad (2)$$

$$\Delta^{199}\mathrm{Hg} = \delta^{199}\mathrm{Hg}_{\mathrm{observed}} - \delta^{199}\mathrm{Hg}_{\mathrm{predicted}} = \delta^{199}\mathrm{Hg}_{\mathrm{observed}} - (\delta^{202}\mathrm{Hg} \times 0.252) \qquad (3)$$

$$\Delta^{201}\mathrm{Hg} = \delta^{201}\mathrm{Hg}_{\mathrm{observed}} - \delta^{201}\mathrm{Hg}_{\mathrm{predicted}} = \delta^{201}\mathrm{Hg}_{\mathrm{observed}} - (\delta^{202}\mathrm{Hg} \times 0.752) \qquad (4)$$

Table S-4 : Hg isotopic composition in reference materials and secondary standard used for method validation, on Mc-ICP-MS. Results are expressed as mean values ± 2SD (standard deviation).

	$^{204/198}\delta$ (‰)	$^{202/198}\delta$ (‰)	$^{201/198}\delta$ (‰)	$^{200/198}\delta$ (‰)	$^{199/198}\delta$ (‰)	Δ201 (‰)	Δ200 (‰)	Δ199 (‰)	n
UM-Almaden	-0,79 ± 0,16	-0,51 ± 0,13	-0,44 ± 0,14	-0,26 ± 0,11	-0,17 ± 0,12	-0,06 ± 0,08	0,00 ± 0,08	-0,04 ± 0,10	31
Fish BCR 464	0,91 ± 0,43	0,69 ± 0,23	2,32 ± 0,41	0,44 ± 0,17	2,39 ± 0,35	1,80 ± 0,24	0,10 ± 0,07	2,22 ± 0,29	4
DOLT 4	-0,39 ± 0,34	-0,22 ± 0,18	0,67 ± 0,18	-0,09 ± 0,16	0,95 ± 0,15	0,84 ± 0,16	0,03 ± 0,09	1,01 ± 0,12	7

Table S-5: Physical parameters for each sampling site. Data is extracted from www.climatedata.eu for all sites except BS for which we used www.weatherbase.com.

	Latitude (° N)	Average annual hours of sunshine (hours)	Annual precipitation (mm)
Agean Sea	40.93	2472	397
North sea	52.06	1765	712
Seine Estuary	49.44	1622	719
Black sea	41.97	1981	682
Northern Adriatic Sea	45.70	2111	1047
Rio de Aveiro Ref.	40.84	2463	1267
Rio de Aveiro Cont.	40.84	2463	1267

Results and discussion

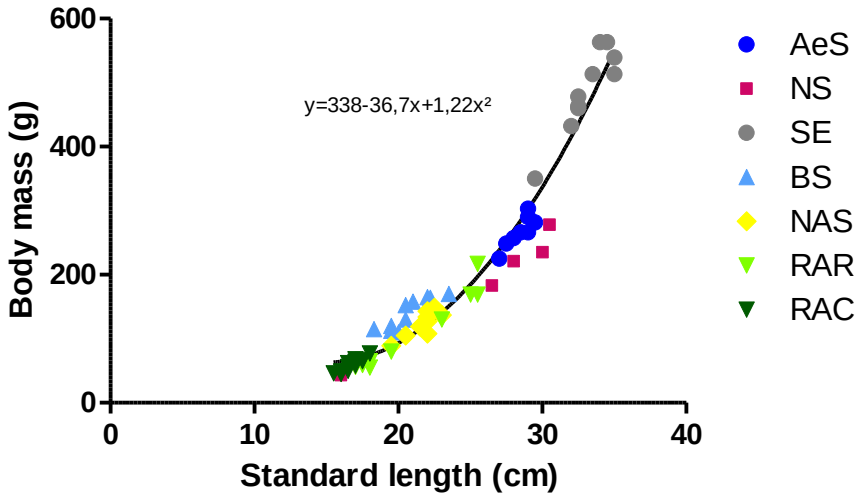

Figure S-2 : Plot of body mass against standard weight of juvenile *Dicentrarchus labrax* sampled across Europe. Best curve fit equation is shown.

Table S-5 : $\delta^{13}C$ and $\delta^{15}N$ values in muscle of *Dicentrarchus labrax.*
All values are expressed as means ± standard deviation (SD), CI…., median (minimum-maximum), n = number of analysed samples

		Agean sea	*North sea*	*Seine Estuary*	*Black sea*	*Northern Adriatic Sea*	*Rio de Aveiro Ref.*	*Rio de Aveiro Cont.*
$\delta^{13}C$	**Mean ± SD**	-18.0 ± 2.0	-16.6 ± 1.3	-17.0 ± 0.7	-21.2 ± 0.4	-18.9 ± 3.2	-17.1 ± 2.6	-17.3 ± 0.8
	95% CI of mean	-19.4 ; -16.6	-18.2 ; -15.1	-17.5 ; -16.5	-21.5 ; -20.9	-21.4 ; -16.5	-18.9 ; -15.2	-17.8 ; -16.8
	Median (Min_Max)	*-17.8 (-22.8 ; -15.8)*	*-16.8 (-17.7 ; -14.5)*	*-17.1 (-18.0 ; -15.3)*	*-21.2 (-22.0 ; -20.6)*	*-17.4 (-24.9 ; -15.3)*	*-16.6 (-24.0 ; -15.0)*	*-17.5 (-18.6 ; -15.6)*
	N	10	5	10	10	9	10	12
$\delta^{15}N$	**Mean ± SD**	11.2 ± 0.8	17.0 ± 1.3	16.9 ± 1.4	10.4 ± 0.2	14.3 ± 1.5	17.4 ± 2.1	18.9 ± 1.1
	95% CI of mean	10.7-11.8	15.4-18.6	15.3-17.3	10.2-10.5	13.1-15.4	15.9-19.0	18.2-19.5
	Median (Min ; Max)	*10.8 (10.5 ; 12.5)*	*17.8 (15.1 ; 18.0)*	*15.8 15.2 ; 20.0)*	*10.4 (10.1 ; 10.8)*	*14.3 (12 ; 16.4)*	*17.0 (15.3 ; 21.1)*	*18.6 (17.6 ; 20.8)*
	N	10	5	10	10	9	10	12

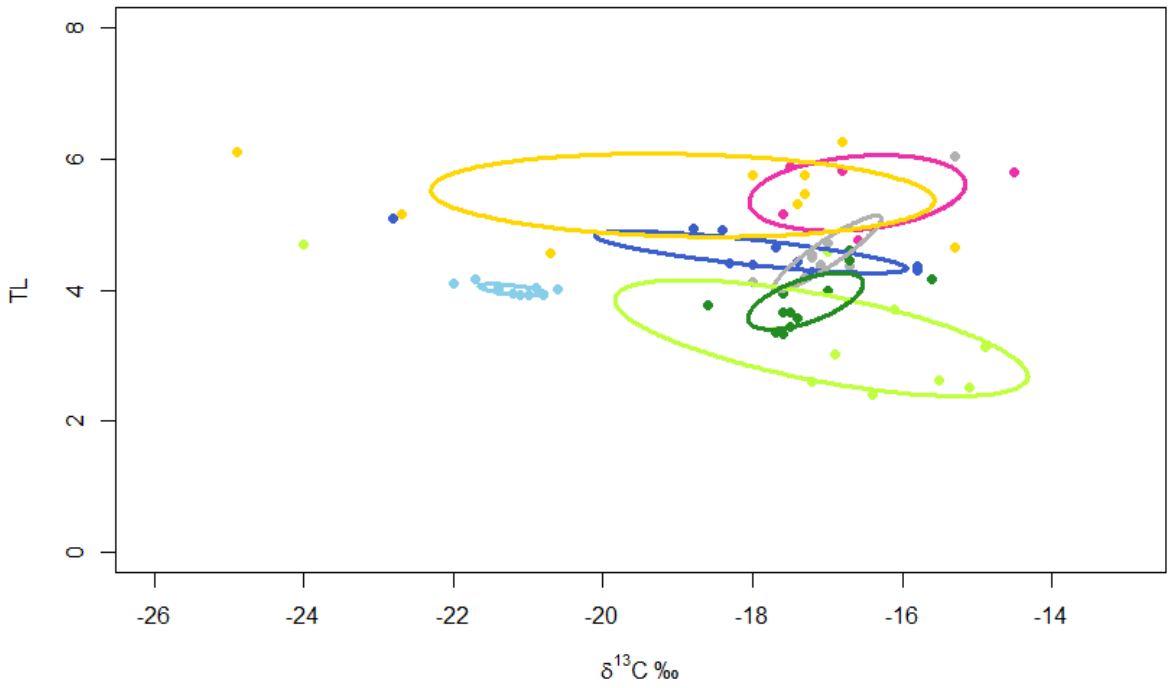

Figure S-3: Trophic niches (TL and $\delta^{13}C$) of *Dicentrarchus labrax* from 7 sampling sites across Europe: the Aegean Sea (AeS), the North Sea (NS), the Seine estuary (SE), the Northern Adriatic Sea (NAS), the Black Sea (BS), and two different sites at the Ria de Aveiro lagoon in Portugal: the reference site, RAR and the contaminated site RAC. Solid lines represent the bivariate standard ellipses associated to each population (through SIBER). Dots represent each individual.

Table S-7: Means ± standard deviation (when available) of $\delta^{15}N$ values in ‰ measured in samples of *Dicentrarchus labrax* muscles, values found in literature for trophic baseline in each sampling site, and λ (estimated baseline trophic level) used in the calculation of trophic level (TL).

	$\delta^{15}N_{samples}$	$\delta^{15}N_{baseline}$	baseline	Source	λ	TL
Agean Sea	11.2 ± 0.8	3,4 ± 0,6	POM	Hannides *et al.* 2015[16]	1,5	4,6
North sea	17.0 ± 1.3	8.12 ± 0.01	*Crassostrea gigas*	Dubois *et al.* 2007[17]	2	5,5
Seine Estuary	16.9 ± 1.4	9,77	*Crassostrea gigas*	Lefebvre *et al.* 2009[18]	2	4,6
Black sea	10.4 ± 0.2	4	POM	Fry *et al.* 1991[19]	1,5	4,0
Northern Adriatic Sea	14.3 ± 1.5	4,5	*Mytilus galloprovincialis*	Kristan *et al.* 2014[20]	2	5,5
Rio de Aveiro Ref.	17.4 ± 2.1	14.2 ± 0.4	*Scrobicularia plana*	Coelho *et al.* 2013[21]	2	3,3
Rio de Aveiro Cont.	18.9 ± 1.1	14.2 ± 0.4	*Scrobicularia plana*	Coelho *et al.* 2013[21]	2	3,8

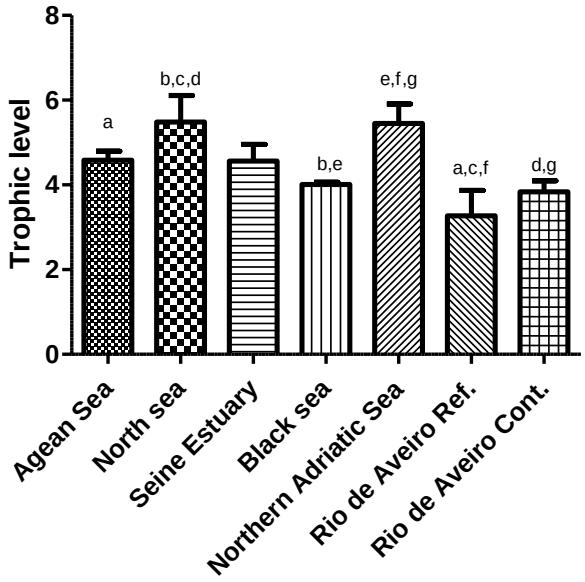

Figure S-4 : Trophic level estimation (means and 95% CI) of Dicentrarchus labrax. The same letter on different sampling sites indicates a p<0.05 after Dunn's multiple comparison test.

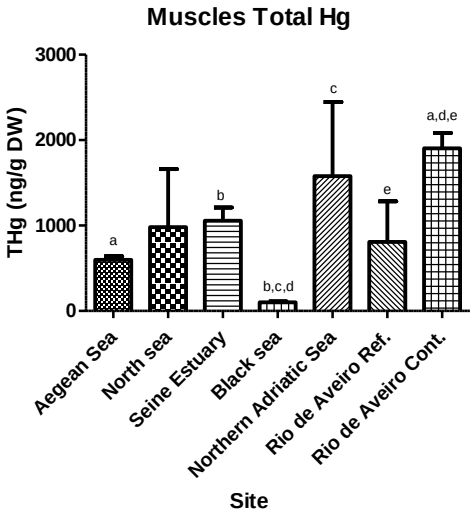

Figure S-5 : Total mercury concentration (ng·g-1 of dry weight), measured in muscle of *Dicentrarchus labrax* from 7 sampling sites across Europe. Significant difference between two sites is indicated by the same letter on the CI bars of the two sites (p<0.05 after Dunn's multiple comparison test)

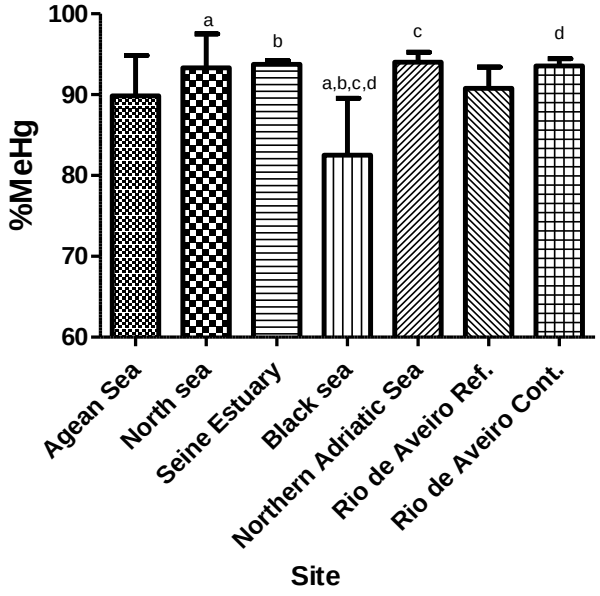

Figure S-6 : Percentage of methylmercury in total Hg, measured in muscle of Dicentrarchus labrax from 7 sampling sites across Europe. Significant difference between two sites is indicated by the same letter on the CI bars of the two sites (p<0.05 after Dunn's multiple comparison test). Data are expressed as mean and 95% CI.

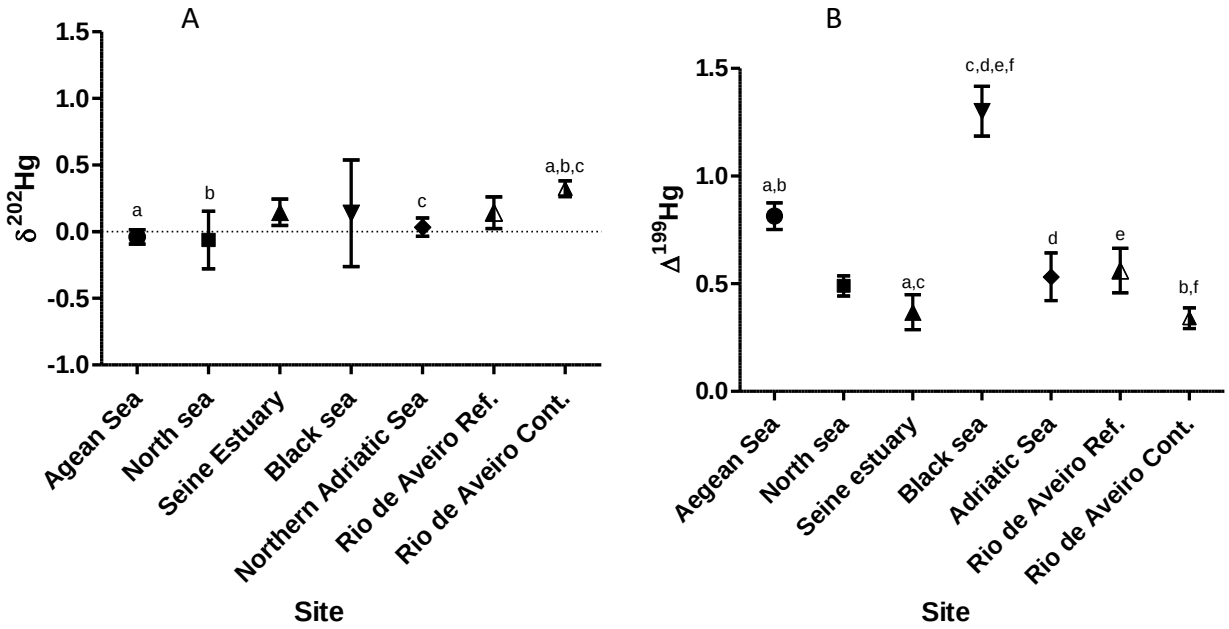

Figure S-7: δ^{202}Hg 5 (A) and Δ^{199}Hg (B) values (‰) measured in muscle of Dicentrarchus labrax from 7 sampling sites across Europe. Significant difference between two sites is indicated by the same letter on the CI bars of the two sites (p<0.05 after Dunn's multiple comparison test). (Kruskal-Wallis test : H=51.02; p<0.0001). Data are expressed as mean and 95% CI.

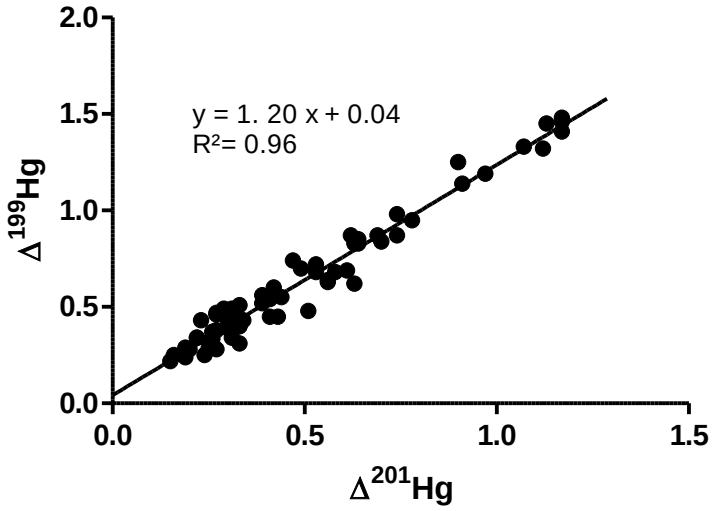

Figure S-7 : Plot of Δ^{199}Hg value versus Δ^{201}Hg value (‰) in muscles of *Dicentrarchus labrax* from 7 sampling sites across Europe, with line showing the regression line for all samples. Value of the slope suggests mass-independent fractionation of Hg in such samples comes from accumulation of photodemethylated MeHg (Spearman correlation; p<0.0001).

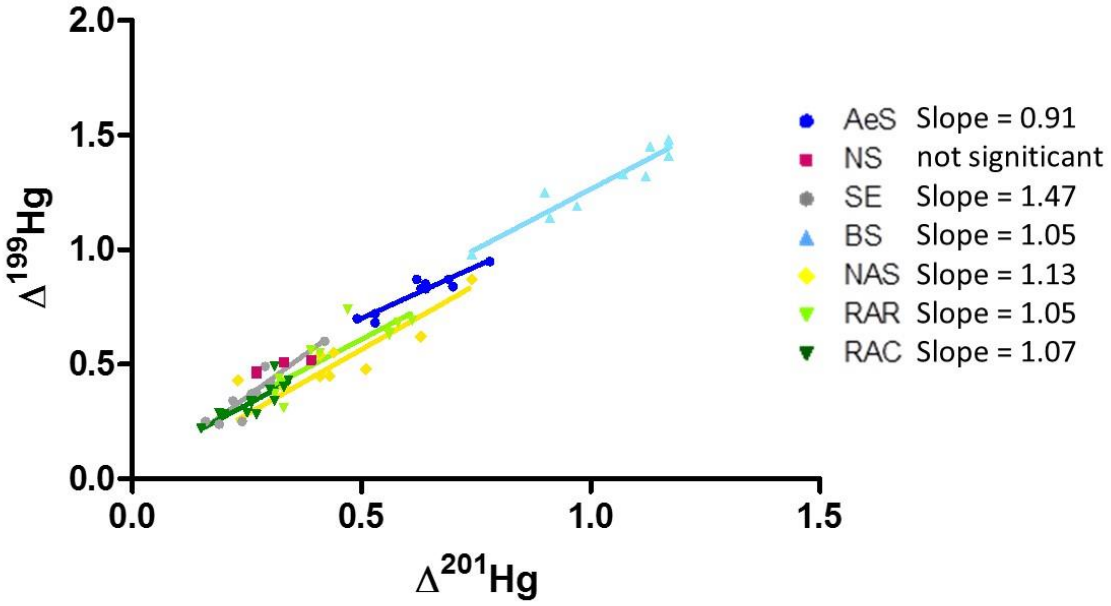

Figure S-9 : Plot of Δ^{199}Hg value versus Δ^{201}Hg value (‰) in muscles of Dicentrarchus labrax from 7 sampling sites across Europe, showing regression line for each sampling site (slope are significantly non-zero, p<0.05). The overall slope for all samples together is 1.20.

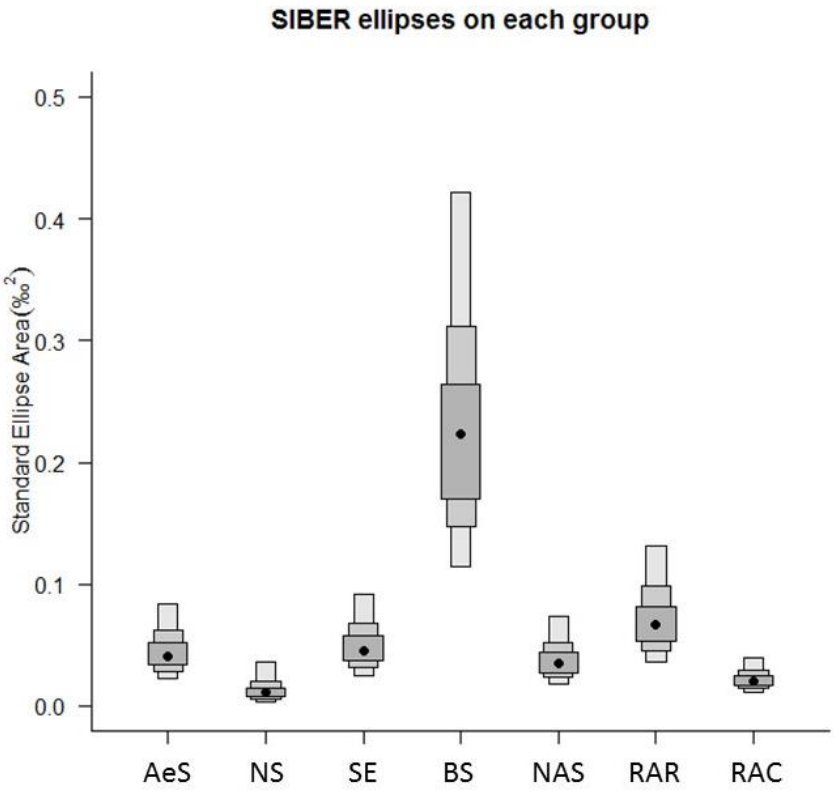

Figure S-10 : Boxplots of model-estimated bivariate standard ellipse area (SEA) associated with the Hg isotopic niches of *Dicentrarchus labrax* from 7 sampling sites across Europe: the Aegean Sea (AeS), the North Sea (NS), the Seine estuary (SE), the Northern Adriatic Sea (NAS), the Black Sea (BS), and two different sites at the Ria de Aveiro lagoon in Portugal: the reference site, RAR and the contaminated site RAC (also see Figure 6). Dark, median and light grey boxes are respectively the 50%, 75% and 95% credibility intervals of the probability of density function distributions of the model solutions, and black dots are the modes of these distributions.

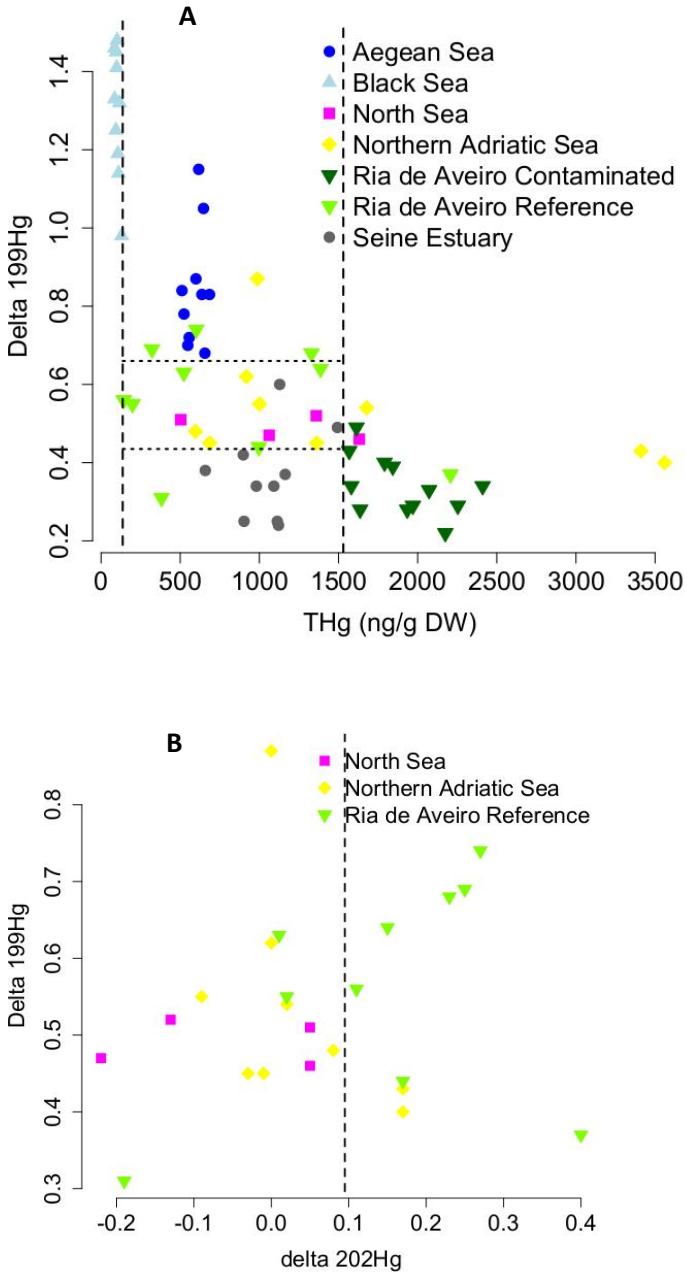

Figure S-11 : (A) and (B) Representation of the nodes that lead to the class boundaries determined in our recursive partitioning analyses.

Table S-8 : least-squares mean THg concentration (lsmean) for each site, accounting for size using the lsmeans function in R, Standard error (SE), degrees of freedom (df), and 95% confidence interval (CL). Standard length=23.42 cm. Results are given on the log (not the response) scale.

Sampling_site	lsmean	SE	df	lower 95CL	upper 95CL
Aegean Sea	6.30	0.98	50	4.34	8.27
Black Sea	4.66	0.29	50	4.07	5.26
North Sea	6.45	0.22	50	6.01	6.90
Northern Adriatic Sea	7.32	0.29	50	6.73	7.92
Ria de Aveiro Contaminated	8.08	1.23	50	5.61	10.56
Ria de Aveiro Reference	6.71	0.18	50	6.35	7.07
Seine Estuary	6.35	0.86	50	4.63	8.07

Table S-9 : least-squares mean MeHg concentration (lsmean) for each site, accounting for size using the lsmeans function in R, Standard error (SE), degrees of freedom (df), and 95% confidence interval (CL). Standard length=23.54 cm. Results are given on the log (not the response) scale.

Sampling_site	lsmean	SE	df	lower 95CL	upper 95CL
Aegean Sea	6.09	0.97	49	4.12	8.04
Black Sea	4.47	0.31	49	3.85	5.10
North Sea	5.55	0.76	49	4.01	7.08
Northern Adriatic Sea	6.99	0.31	49	6.36	7.63
Ria de Aveiro Contaminated	7.79	1.28	49	5.22	10.36
Ria de Aveiro Reference	6.48	0.18	49	6.11	6.85
Seine Estuary	6.28	0.86	49	4.54	8.01

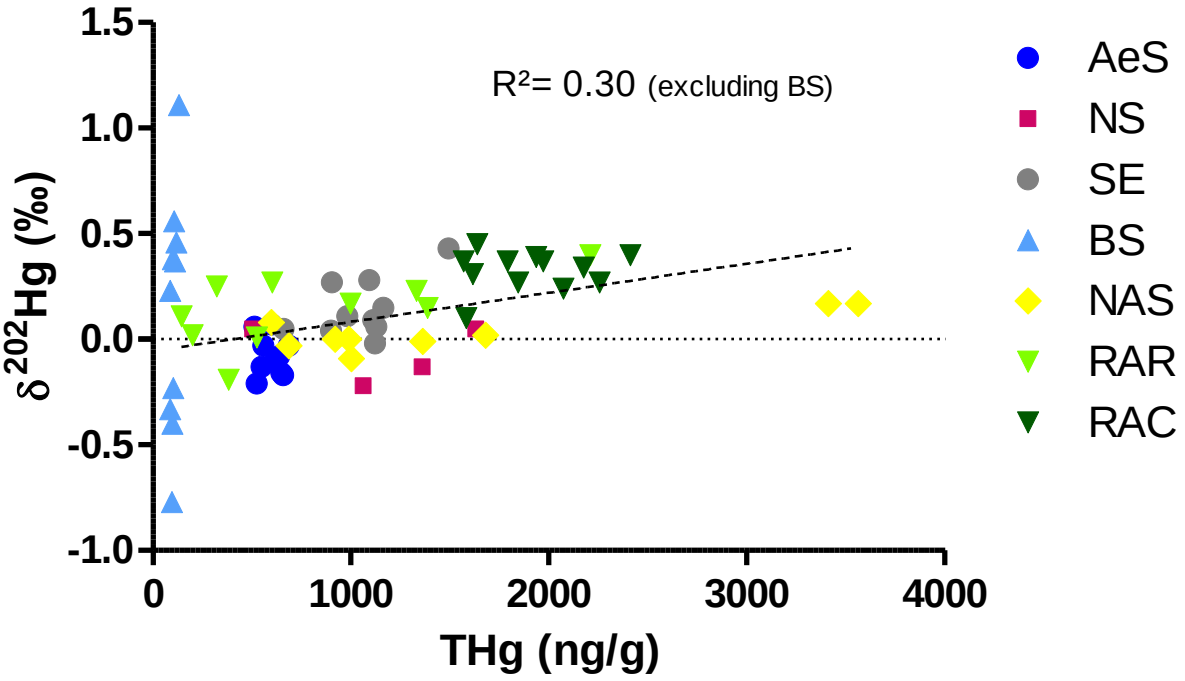

Figure S-12 : Total Hg concentration versus δ^{202}Hg in muscle tissue of *Dicentrarchus labrax* from 7 sampling sites across Europe: the Aegean Sea (AeS), the North Sea (NS), the Seine estuary (SE), the Northern Adriatic Sea (NAS), the Black Sea (BS), and two different sites at the Ria de Aveiro lagoon in Portugal: the reference site, RAR and the contaminated site RAC. The regression line for all samples except BS is shown. Dots represent individuals

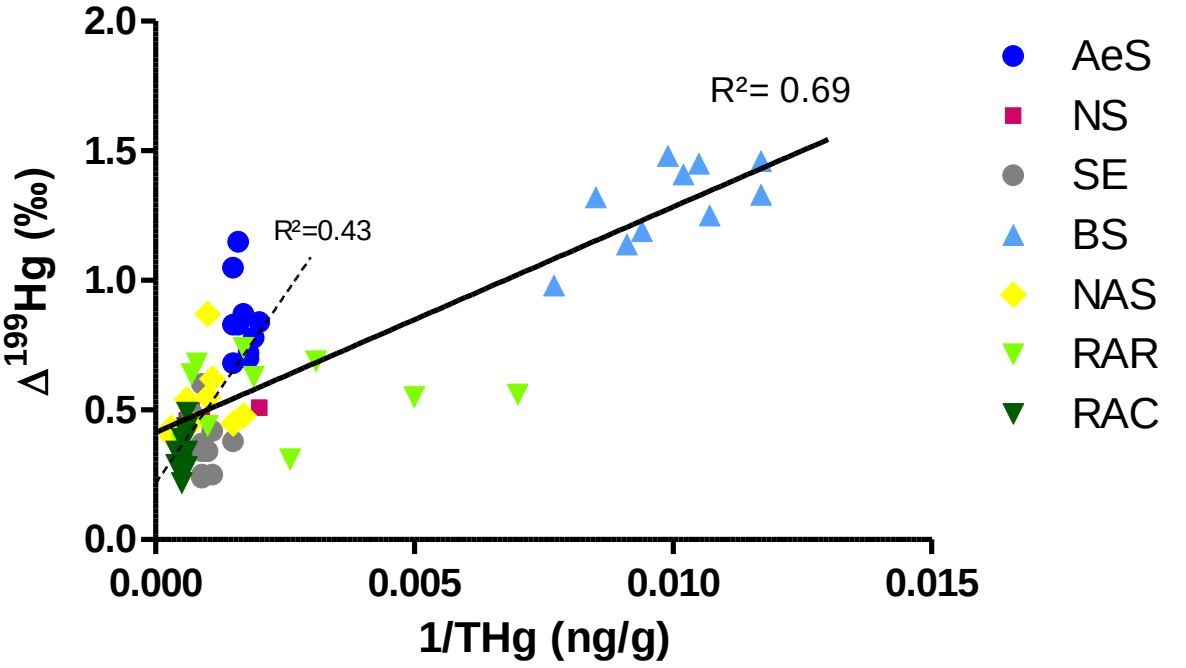

Figure S-13 : Total Hg concentration versus Δ199Hg in muscle tissue of *Dicentrarchus labrax* from 7 sampling sites across Europe: the Aegean Sea (AeS), the North Sea (NS), the Seine estuary (SE), the Northern Adriatic Sea (NAS), the Black Sea (BS), and two different sites at the Ria de Aveiro lagoon in Portugal: the reference site, RAR and the contaminated site RAC. Continuous line represents the regression line for all points and the dotted line is the regression without BS and RAR points.

Supplementary discussion on MIF values, and their link with MeHg from coastal versus pelagic sources

Lower MIF values have been associated to MeHg produced in coastal areas, whereas higher MIF values have been associated to relatively more oceanic/pelagic produced MeHg[25–27]. MIF observed in our samples ranged between values reported in other studies (Figure S-14). Lower values that were measured at SE, NAS, RAR and RAC are similar to those observed in coastal marine biota in previous studies[27,25,26] and could be linked with low water clarity from high suspended sediment loads and high primary production relative to oceanic waters. The higher MIF values that we found in AeS and in BS samples could be related to higher water clarity and greater light penetration that would allow faster photochemical MeHg degradation rates, such as has been clearly observed in pelagic waters. AeS values were still consistent with previously reported data for coastal fish[25–27].

Supplementary discussion on MDF for each sampling site

In previous studies on marine environment, the extent of the isotopic δ^{202}Hg offset between sediment THg and fish THg was estimated around 0.73 ‰ (± 0.16 ‰ 1SD)[26] and 0.66 ‰(± 0.25 ‰ 1SD)[27]. In the present work, we didn't sample sediment and are consequently unable to precisely measure the δ^{202}Hg offset. Yet, the sediment Hg isotopic composition of one of our sampling sites, NAS, has been previously characterized: contaminated sediments of the Gulf of Trieste had a mean δ^{202}Hg of -0.36 ‰ (± 0.09 ‰ 1SD)[9]. The δ^{202}Hg of our NAS samples was 0.03 ‰ on average (± 0.09 ‰ 1SD), corresponding to an estimated offset of 0.39 ‰ which is in accordance with one study[27]. Thus in NAS, the hypothesis that MeHg in biota originates from sediment THg would be consistent. Furthermore, the Δ^{199}Hg/Δ^{201}Hg slope of 1.13 is coherent with a photodemethylation of MeHg, which would cause a positive offset between fish and sediment.

In RAC site, the pollution source absolute δ^{202}Hg values (from chloralkali) would probably have shifted due to Hg cycling in sediment, leading to a probable offset between sediment and fish, as discussed above. This offset, however, is not quantifiable in the present state of our knowledge. The low MIF value and low MIF slope suggest that MeHg photodemethylation would not be important at this site.

The wide range of THg concentrations and the seemingly corresponding δ^{202}Hg gradient (Figure S-12) at RAR site suggest that seabass from this site present THg and δ^{202}Hg values varying between actual background levels and RAC site levels and δ^{202}Hg. Nevertheless, the core Hg isotopic niche of RAR seabass is clearly distinct from the RAC Hg isotopic niche (Figure 1). The RAR site would thus not exactly be a reference site as suggested in previous work but a heterogeneous site that could rather be considered as an intermediate site between an actual background site and RAC site.

The SE seabass characteristics (high THg, low MIF with a 1.47 slope (Figure 1 and S-9) and intermediate δ^{202}Hg) suggest an important and regular local input of Hg with a δ^{202}Hg that would be distinct from the background δ^{202}Hg, but not as much as in RAC site. The SE site is a well-known metal contaminated areas due intensive industrial activity. The world's biggest Hg mining district happens to be Almaden, in Spain. It is likely to have been providing many European industries with Hg and its δ^{202}Hg has been estimated to be around -0.5 ‰[28,29]. An offset between sediments having a -0.5 ‰ δ^{202}Hg and SE seabass would be around 0.65 ‰, which coincides

with previously observed offset [26,27]. This could suggest the contamination source in SE to be linked with industrial mercury originating from the Mediterranean basin. This is of course speculative, but still coherent with our findings.

We were not able to bring out any correlation between δ^{202}Hg in fish muscle and some factors that may influence it (latitude, annual hours of sunshine and annual precipitation). This is most probably due to varying Hg sources with different δ^{202}Hg values between sites as discussed in the previous paragraphs, and to varying offsets between sites. The link between δ^{202}Hg offset (sediment THg – biota MeHg) and physical parameters would be worth investigating.

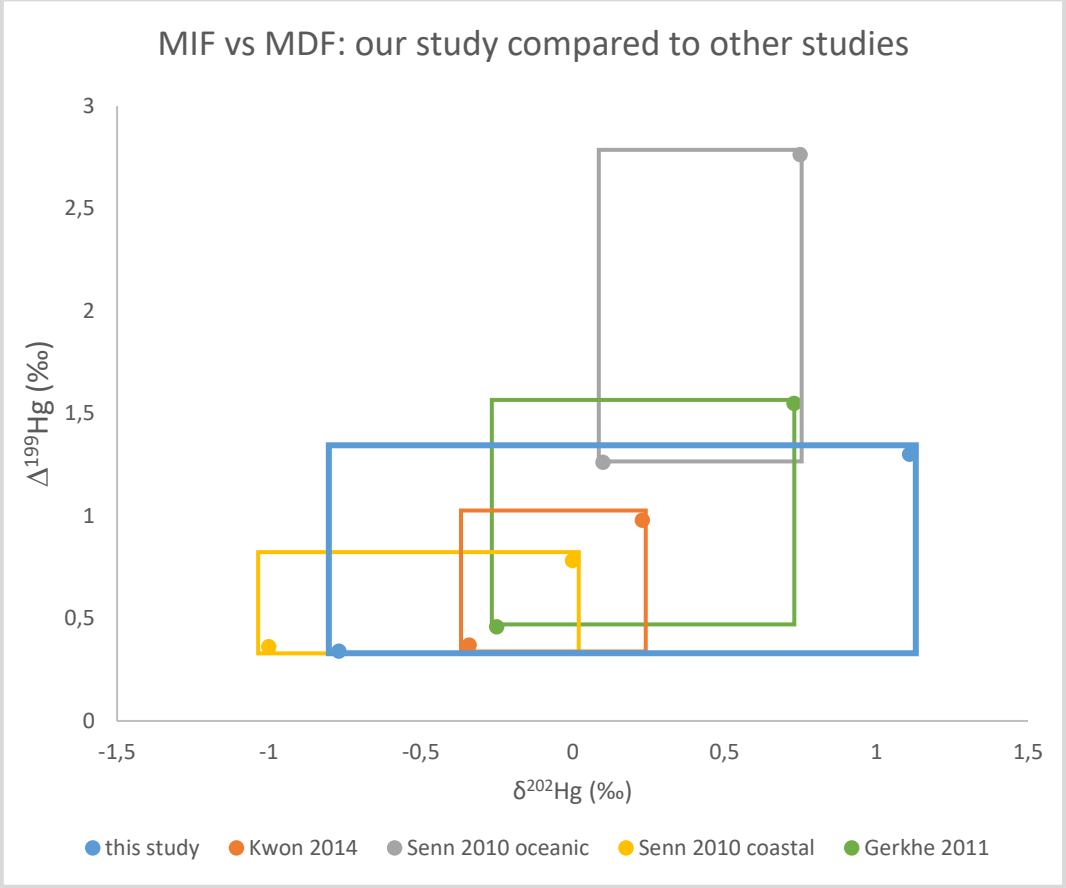

Figure S-14 : MDF (δ^{202}Hg) and MIF (Δ^{199}Hg) values measured in the present study and other studies[25,27,30].

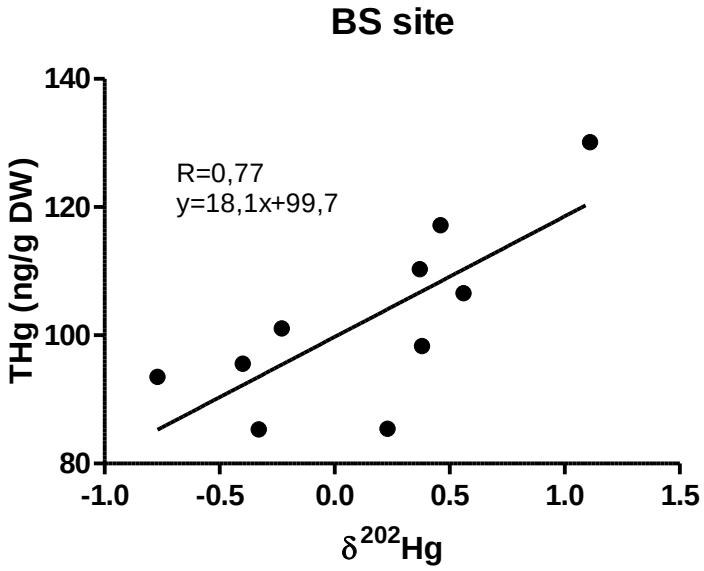

Figure S-15 : THg concentration (ng·g^{-1} DW) versus δ^{202}Hg value (‰) measured in muscle of *Dicentrarchus labrax* from the Black Sea.

Previous studies have suggested that demethylation of MeHg might take place in fish liver as a detoxifying mechanism[31,32], like has been demonstrated in other organisms. Our results showed a negative relationship between THg and %MeHg in BS, as well as significant positive relationship between THg and δ^{202}Hg (Figure S-15). This would be consistent with an increasing demethylation of MeHg as THg concentration rise in fish. We hypothesize that demethylation of MeHg in fish would induce MDF, like any biological process, and that the extent of *in vivo* demethylation and subsequent MDF would be a good source of δ^{202}Hg variation as observed in BS site. Such variation would only be observed in BS population because its THg contamination is particularly low compared to the other populations.

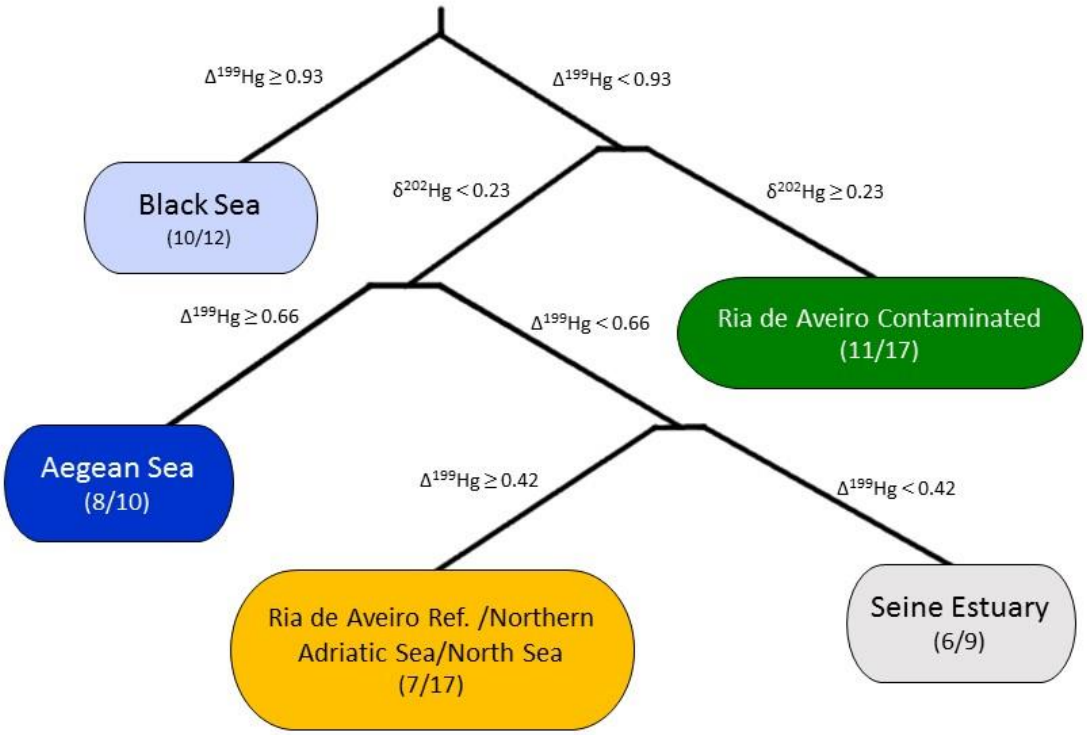

Figure S-16 : **Classification** tree for Hg variables in populations of *Dicentrarchus labrax*, after recursive partitioning analysis (n=65), using only δ^{202}Hg and Δ^{199}Hg

References:

(1) OSPAR Commission. *Quality status report 2010*; The Commission, 2010.

(2) Tappin, A. D.; Millward, G. E. The English Channel: Contamination status of its transitional and coastal waters. *Mar. Pollut. Bull.* **2015**, *95* (2), 529–550.

(3) Christophoridis, A. .; Stamatis, N. .; Orfanidis, S. . Sediment heavy metals of a mediterranean coastal lagoon: Agiasma, nestos delta, eastern macedonia (greece). *Transitional Waters Bull.* **2007**, *1* (4), 33–43.

(4) Andreev, G. Distribution of mercury in the open-sea region of the South-Western Black Sea. *Toxicol. Environ. Chem.* **1987**, *16* (1), 75–80.

(5) Akbal, F.; Gürel, L.; Bahadır, T.; Güler, İ.; Bakan, G.; Büyükgüngör, H. Water and sediment quality assessment in the mid-Black Sea coast of Turkey using multivariate statistical techniques. *Environ. Earth Sci.* **2011**, *64* (5), 1387–1395.

(6) Sorokin, Y. U. I. The Black Sea. In *Etuaries and Enclosed Seas: Ecosystems of the World*; Elsevier, Ed.; Amsterdam, 1983; pp 253–291.

(7) Lamborg, C. H.; Yiğiterhan, O.; Fitzgerald, W. F.; Balcom, P. H.; Hammerschmidt, C. R.; Murray, J. Vertical distribution of mercury species at two sites in the Western Black Sea. *Mar. Chem.* **2008**, *111* (1–2), 77–89.

(8) Capet, A.; Stanev, E. V; Beckers, J.-M.; Murray, J. W.; Grégoire, M. Decline of the Black Sea oxygen inventory. *Biogeosciences* **2016**, *13* (4), 1287–1297.

(9) Foucher, D.; Hintelmann, H. Tracing mercury contamination from the Idrija mining region (Slovenia) to the Gulf of Trieste using Hg isotope ratio measurements. *Environ. Sci. Technol.* **2008**, *43* (1), 33–39.

(10) Acquavita, A.; Covelli, S.; Emili, A.; Berto, D.; Faganeli, J.; Giani, M.; Horvat, M.; Koron, N.; Rampazzo, F. Mercury in the sediments of the Marano and Grado Lagoon (northern Adriatic Sea): Sources, distribution and speciation. *Estuar. Coast. Shelf Sci.* **2012**, *113*, 20–31.

(11) Mieiro, C.; Pacheco, M.; Pereira, M.; Duarte, A. Mercury Organotropism in Feral European Sea Bass *(Dicentrarchus labrax*). *Arch. Environ. Contam. Toxicol.* **2011**, *61* (1), 135–143.

(12) Coelho, J. P.; Pereira, M. E.; Duarte, A.; Pardal, M. A. Macroalgae response to a mercury contamination gradient in a temperate coastal lagoon (Ria de Aveiro, Portugal). *Estuar. Coast. Shelf Sci.* **2005**, *65* (3), 492–500.

(13) Post, D. M. Using stable isotopes to estimate trophic position: models, methods, and assumptions. *Ecology* **2002**, *83* (3), 703–718.

(14) Barnes, C.; Jennings, S.; Polunin, N. V. C.; Lancaster, J. E. The importance of quantifying inherent variability when interpreting stable isotope field data. *Oecologia* **2007**, *155* (2), 227–235.

(15) Vanderklift, M. A.; Ponsard, S. Sources of variation in consumer-diet $\delta^{15}N$ enrichment: a meta-analysis. *Oecologia* **2003**, *136* (2), 169–182.

(16) Hannides, C. C. S.; Zervoudaki, S.; Frangoulis, C.; Lange, M. A. Mesozooplankton stable isotope composition in Cyprus coastal waters and comparison with the Aegean Sea (eastern Mediterranean). *Estuar. Coast. Shelf Sci.* **2015**, *154*, 12–18.

(17) Dubois, S.; Jean-Louis, B.; Bertrand, B.; Lefebvre, S. Isotope trophic-step fractionation of suspension-feeding species: Implications for food partitioning in coastal ecosystems. *J. Exp. Mar. Bio. Ecol.* **2007**, *351* (1–2), 121–128.

(18) Lefebvre, S.; Harma, C.; Blin, J. L. Trophic typology of coastal ecosystems based on $\delta^{13}C$ and $\delta^{15}N$ ratios in an opportunistic suspension feeder. *Mar Ecol Prog Ser* **2009**, *390*, 27–37.

(19) Fry, B.; Jannasch, H. W.; Molyneaux, S. J.; Wirsen, C. O.; Muramoto, J. A.; King, S. Stable isotope studies of the carbon, nitrogen and sulfur cycles in the Black Sea and the Cariaco Trench. *Deep Sea Res. Part A. Oceanogr. Res. Pap.* **1991**, *38*, S1003–S1019.

(20) Kristan, U.; Kanduč, T.; Osterc, A.; Šlejkovec, Z.; Ramšak, A.; Stibilj, V. Assessment of pollution level using Mytilus galloprovincialis as a bioindicator species: The case of the Gulf of Trieste. *Mar. Pollut. Bull.* **2014**, *89* (1–2), 455–463.

(21) Coelho, J. P.; Mieiro, C. L.; Pereira, E.; Duarte, A. C.; Pardal, M. A. Mercury biomagnification in a contaminated estuary food web: effects of age and trophic position using stable isotope analyses. *Mar. Pollut. Bull.* **2013**, *69* (1–2), 110–115.

(22) Lorrain, A.; Graham, B. S.; Popp, B. N.; Allain, V.; Olson, R. J.; Hunt, B. P. V.; Potier, M.; Fry, B.; Galván-Magaña, F.; Menkes, C. E. R.; et al. Nitrogen isotopic baselines and implications for estimating foraging habitat and trophic position of yellowfin tuna in the Indian and Pacific Oceans. *Deep Sea Res. Part II Top. Stud. Oceanogr.* **2015**, *113*, 188–198.

(23) McCarthy, M. D.; Benner, R.; Lee, C.; Fogel, M. L. Amino acid nitrogen isotopic fractionation patterns as indicators of heterotrophy in plankton, particulate, and dissolved organic matter. *Geochim. Cosmochim. Acta* **2007**, *71* (19), 4727–4744.

(24) Rodríguez Martín-Doimeadios, R. C.; Krupp, E.; Amouroux, D.; Donard, O. F. X. Application of Isotopically Labeled Methylmercury for Isotope Dilution Analysis of Biological Samples Using Gas Chromatography/ICPMS. *Anal. Chem.* **2002**, *74* (11), 2505–2512.

(25) Senn, D. B.; Chesney, E. J.; Blum, J. D.; Bank, M. S.; Maage, A.; Shine, J. P. Stable isotope (N, C, Hg) study of methylmercury sources and trophic transfer in the Northern Gulf of Mexico. *Environ. Sci. Technol.* **2010**, *44* (5), 1630–1637.

(26) Gehrke, G. E.; Blum, J. D.; Slotton, D. G.; Greenfield, B. K. Mercury Isotopes Link Mercury in San Francisco Bay Forage Fish to Surface Sediments. *Environ. Sci. Technol.* **2011**, *45* (4), 1264–1270.

(27) Kwon, S. Y.; Blum, J. D.; Chen, C. Y.; Meattey, D. E.; Mason, R. P. Mercury Isotope Study of Sources and Exposure Pathways of Methylmercury in Estuarine Food Webs in the Northeastern U.S. *Environ. Sci. Technol.* **2014**, *48* (17), 10089–10097.

(28) Wiederhold, J. G.; Skyllberg, U.; Drott, A.; Jiskra, M.; Jonsson, S.; Björn, E.; Bourdon, B.; Kretzschmar, R. Mercury isotope signatures in contaminated sediments as a tracer for local industrial pollution sources. *Environ. Sci. Technol.* **2015**, *49* (1), 177–185.

(29) Gray, J. E.; Pribil, M. J.; Higueras, P. L. Mercury isotope fractionation during ore retorting in the Almadén mining district, Spain. *Chem. Geol.* **2013**, *357*, 150–157.

(30) Gehrke, G. E.; Blum, J. D.; Marvin-DiPasquale, M. Sources of mercury to San Francisco Bay surface sediment as revealed by mercury stable isotopes. *Geochim. Cosmochim. Acta* **2011**, *75* (3), 691–705.

(31) Gonzalez, P.; Dominique, Y.; Massabuau, J. C.; Boudou, A.; Bourdineaud, J. P. Comparative Effects of Dietary Methylmercury on Gene Expression in Liver, Skeletal Muscle, and Brain of the Zebrafish (*Danio rerio*). *Environ. Sci. Technol.* **2005**, *39* (11), 3972–3980.

(32) Feng, C.; Pedrero, Z.; Gentès, S.; Barre, J.; Renedo, M.; Tessier, E.; Berail, S.; Maury-Brachet, R.; Mesmer-Dudons, N.; Baudrimont, M.; et al. Specific Pathways of Dietary Methylmercury and Inorganic Mercury Determined by Mercury Speciation and Isotopic Composition in Zebrafish (*Danio rerio*). *Environ. Sci. Technol.* **2015**, *49* (21), 12984–12993.